JACS
JOURNAL OF THE AMERICAN CHEMICAL SOCIETY
Article
pubs.acs.org/JACS

# Geometries, Electronic Couplings, and Hole Dissociation Dynamics of Photoinduced Electron−Hole Pairs in Polyhexylthiophene−Fullerene Dyads Rigidly Linked by Oligophenylenes

Taku Miura,[†] Ran Tao,[‡] Sho Shibata,[‡] Tomokazu Umeyama,[‡] Takashi Tachikawa,[†] Hiroshi Imahori,[*,‡,#] and Yasuhiro Kobori[*,†]

[†]Department of Chemistry, Graduate School of Science, Kobe University, 1-1 Rokkodaicho, Nada-ku, Kobe 657-8501, Japan
[‡]Department of Molecular Engineering, Graduate School of Engineering, Kyoto University, Nishikyo-ku, Kyoto 615-8510, Japan
[#]Institute for Integrated Cell-Material Sciences (WPI-iCeMS), Kyoto University, Nishikyo-ku, Kyoto 615-8510, Japan

Supporting Information

**ABSTRACT:** To shed a light on fundamental molecular functions of photoinduced charge conductions by organic photovoltaic materials, it is important to directly observe molecular geometries of the intermediate charges just after the photoinduced electron-transfer reactions. However, highly inhomogeneous molecular environments at the bulk heteojunction interfaces in the photoactive layers have prevented us from understanding the mechanism of the charge conductions. We have herein investigated orbital geometries, electronic couplings, and hole-dissociation dynamics of photoinduced charge-separated (CS) states in a series of poly(3-hexylthiophene)−fullerene linked dyads bridged by rigid oligo-*p*-phenylene spacers by using time-resolved EPR spectroscopy. It has been revealed that one-dimensional intramolecular hole-dissociations exothermically take place from localized holes in initial CS states, following bridge-mediated, photoinduced charge-separations via triplet exciton diffusions in the conjugated polymer-backbones. This molecular wire property of the photoinduced charges in solution at room temperature demonstrates the potential utility of the covalently bridged polymer molecules applied for the molecular devices.

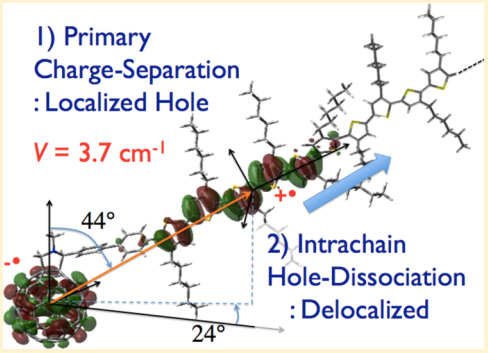


## INTRODUCTION

For developments of the organic light-energy conversion systems, it is essential to achieve efficient long-range charge-separations (CS). Light-induced electrons and holes generated by the electron-transfer (ET) reactions are thus required to escape from the electrostatic binding at the initial stage. In the natural photosynthetic reaction centers, the efficient distant CS is accomplished with ∼100% efficiency by cascading the redox states by the sequential ET processes to a series of cofactors, leading to the light-to-chemical energy conversion.[1] In contrast, the photoinduced CS at the interfaces of organic photovoltaic (OPV)[2] cells generates electron−hole pairs, eventually achieving light-to-electricity conversion after conductions of the electron and the hole through the acceptor (A) and the donor (D) domains, respectively. However, the D/A interfaces in the OPV cells often suffer from the charge-recombination (CR) at the early stage,[3] leading to losses of the input photon energies.[4]

Concerning the mechanism of the efficient photocarrier generations in the OPV systems, the role of the hot charge-transfer (CT) excitons is currently under intense debate.[5−7] A recent ultrafast spectroscopic study[8] of a polymer/fullerene (PCPDTBT/$PC_{60}BM$) OPV films clearly showed that the vibrationally unrelaxed electron−hole pairs (PCPDTBT$^{+}$/$PC_{60}BM^{-}$) are generated in <50 fs before time scales of the internal conversions (IC) of the polymer excited states. On the other hand, Vandewal et al.[9] have demonstrated for the several polymer/PCBM solar cells that the internal quantum efficiency (IQE) is essentially independent of the excitation energy of the lights; even if the low-energy CT band is excited, the IQE is higher than 90% for some blend films, giving rise to very high OPV performances. This result strongly indicates that the hot CT states are not necessarily required to produce the highly separated photocarriers. To elucidate why and how the photocarriers escape from the Coulomb binding,[10−14] it is important to directly observe locations and orientations of the intermediate charges just after the CSs. Time-resolved electron paramagnetic resonance (TREPR) and pulsed EPR methods have been powerful[15−23] to obtain the electron spin−spin dipolar interaction ($D'$) and the spin−spin exchange coupling ($J$) in the photoinduced CS states and thus have been utilized to characterize the interspin distances and the electronic couplings ($V$)[12,24,25] of the transient CS states. The TREPR analyses have been useful to obtain the CS state geometries for several systems, since the electron spin polarization (ESP) as

**Received:** December 23, 2015
**Published:** April 15, 2016





DOI: 10.1021/jacs.5b13414
J. Am. Chem. Soc. 2016, 138, 5879−5885

the microwave absorption ($A$) and the emission ($E$) is sensitive to the molecular conformations and to $J$.[12,26−28] Recent spin polarization analyses have revealed representative geometries of the transient electron−hole pairs in the OPV blends.[12,24] However, the highly inhomogeneous molecular environments at the bulk heteojunction (BHJ) interfaces induce the large special distribution in the solid-state OPV materials and would prevent us from understanding the mechanism of the charge conductions.[21,29]

To unveil fundamental molecular mechanisms of the light-induced charge conductions, it is highly desired to investigate the structure and dynamics of the initial photocarriers generated in a conjugated polymer-backbone in which the intramolecular orientation and the electronic interaction are well-defined at the initial CS stage. Thus far, no study has characterized the geometry, electronic coupling, and charge-conduction dynamics of the photocarriers in a covalently linked polymer system, although the polymer−fullerene dyads were synthesized and investigated by transient spectroscopies.[30,31] In this respect, we have synthesized a new series of donor-bridge-acceptor (P3HT-Ph$_m$-C$_{60}$, $m$ = 0, 1, 2, 3) linked polymers composed of regioregular poly(3-hexylthiophene) (P3HT) as the electron donor, fulleropyrrolidine (C$_{60}$) as the acceptor and oligo-$p$-phenylene bridges as the spacers (Figure 1). The rigid

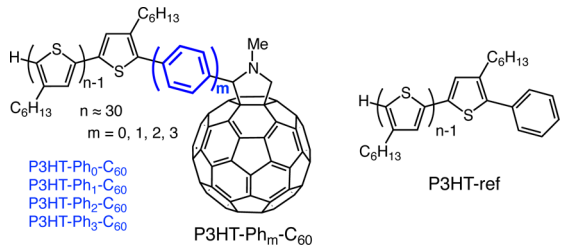


**Figure 1.** Structure formula of P3HT-Ph$_m$-C$_{60}$ and P3HT-ref. Averaged number of $n$ is ≈30 in the P3HT units.

spacers ensure homogeneous properties in the molecular conformations of the polymer-backbone and C$_{60}$ nearby the bridging units. We have herein investigated the molecular geometries and the hole-conduction dynamics of the photo-induced intramolecular CS states by using the TREPR in tetrahydrofuran (THF) at room temperature. We clearly show that, without going through the hot CT, localized holes are generated in the conjugated polymer-backbones nearby the phenylene units by quenching triplet excitons and then undergo one-dimensional intramolecular dissociations from the electrons situated at C$_{60}$ in the dyads.

## RESULTS AND DISCUSSION

**TREPR Measurements.** Figure 2a shows the TREPR spectra for several delay times after the 532 nm irradiations of the P3HT-Ph$_1$-C$_{60}$ dyad in THF at room temperature. A mean concentration of the dyad was $10^{-4}$ M in THF solutions from the averaged molecular weight ≈ 6000 as detailed in the Supporting Information. Measurements of the time-resolved fluorescence decays and the nanosecond transient absorption spectra demonstrated that the triplet excitons of $^3$P3HT*-Ph$_m$-C$_{60}$ are dominantly generated by the intersystem crossing (ISC) of the singlet excitons $^1$P3HT*-Ph$_m$-C$_{60}$, as explained with Figures S7 and S8 in Supporting Information. At the initial stage in Figure 2a, a strong microwave emission ($E$) has been seen with a broad spectrum-width around the resonant field

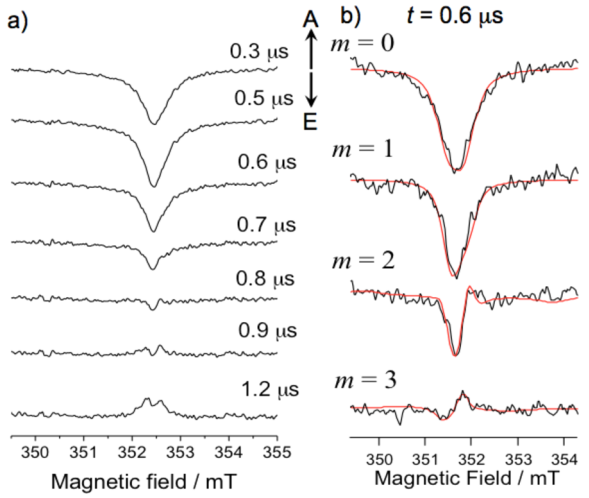


**Figure 2.** (a) Delay time (0.3−1.2 $\mu$s from the top to the bottom) dependence of the TREPR spectrum of P3HT-Ph$_1$-C$_{60}$ in THF at room temperature after the 532 nm laser excitations. (b) Effect of the TREPR spectrum on the phenylene spacer length ($m$) in P3HT-Ph$_m$-C$_{60}$ at 0.6 $\mu$s. The red lines are calculated TREPR spectra at $t$ = 0.6 $\mu$s using the triplet ESPT model of Figure 3.

region for P3HT cation radical ($g_{P3HT}$ ≈ 2.002 as the $g$-factor) and for fulleropyrrolidine anion radical ($g_{C60}$ ≈ 2.000).[32] This net $E$ polarization is explained by the triplet mechanism (TM)[33] by which the spin polarization of the precursor excited triplet state is transferred to the sublevel populations in the spin correlated radical pairs (SCRP) by the electron spin polarization transfer (ESPT) as shown in Figure 3.[34,35] This implies

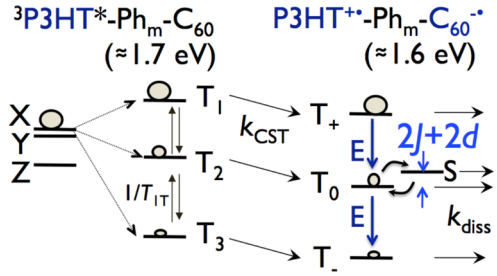


**Figure 3.** (Left) Spin polarization model in the precursor triplet sublevels generated by ISC of $^1$P3HT*-Ph$_m$-C$_{60}$ in the absence (X, Y, Z) and in the presence ($T_1$, $T_2$, $T_3$) of $B_0$. The electronic energy is $E_T$ ≈ 1.7 eV. (Right) Triplet sublevel populations ($T_+$, $T_0$, $T_-$) after ESPT in the primary CS state (energy ≈ 1.6 eV), resulting in the net $E$ polarization detected by the TREPR. Since the spin-state energies of $T_+$, $T_0$ and $T_-$ are dependent on the direction of the interspin vector (orange arrow in Figure 4) in the principal axis system of $X$, $Y$, $Z$ in the ZFS interaction, the TREPR spectrum of the CS state is highly affected by the molecular orientation as shown in Figure 5. The spin−lattice relaxations ($1/T_{1T}$) by the triplet exciton-diffusion are represented by the vertical arrows. $k_{diss}$ (≈ $10^6$ s$^{-1}$) is the hole-dissociation rate constant.

that the hot CT exciton is not involved in the primary CS, since the ISC contributes to the SCRP observations. Interestingly, the broad spectrum-shape is changed by the delay time into two absorptive sharp peaks in Figure 2a. The peak positions (352.2 and 352.6 mT) at the bottom in Figure 2a were consistent with the resonance fields[32,36] of isolated P3HT$^{+\bullet}$ and C$_{60}^{-\bullet}$, respectively, indicating that the holes dissociate from the electrons at the later delay times. Figure 2b shows comparisons


DOI: 10.1021/jacs.5b13414
J. Am. Chem. Soc. 2016, 138, 5879−5885

of the TREPR spectra of P3HT-Ph$_m$-C$_{60}$ for different phenylene spacer lengths ($m$) at the initial delay times of 0.6 $\mu$s. The entire line-width becomes smaller by the increase in $m$. This result is explained by the weakened electron spin dipolar coupling of $D'$ in P3HT$^{+\bullet}$-Ph$_m$-C$_{60}^{-\bullet}$ by the increase in $m$, indicating that the electron and the hole in the electron−hole pair are initially situated in close proximity to the spacer units (−Ph$_m$−). The triplet state energy is reported to be $E_T \approx 1.7$ eV in $^3$P3HT* in a liquid solution.[37] From the redox potentials measured in a mixture solvent of 1,2-dichlorobenzene and acetonitrile ($v$:$v$ = 5:1) in Figure S11, the CS state energy is evaluated to be $-\Delta G_{CR} \approx 1.6$ eV for the dissociated pair of the radical anion and the polaron in THF. This denotes that the CS is exothermic from $^3$P3HT* in Figure 3. Therefore, it is concluded that the bridge-mediated intramolecular CS takes place when the triplet exciton resides nearby the -Ph$_m$- after the triplet-exciton diffusion[38] within the thiophene backbones. For the larger phenylene spacer lengths, the net $E$ polarization becomes weaker and an $E/A$ polarization is observed for $m$ = 3 in Figure 2b. The disappearance of the net $E$ is explained by a larger triplet spin−lattice relaxation rate[39] ($1/T_{1T}$) than the triplet CS rate ($k_{CST}$) in Figure 3, resulting in the thermal equilibrium spin populations in the precursor triplet. For any spacer lengths, similar delay time dependences on the line shape have been obtained as in Figure 2a yielding the absorptive sharp spectra at >1 $\mu$s.

The spacer length dependence on the initial spectrum-width in Figure 2b denotes that the molecular rotations are slow enough, exhibiting the spin dipolar interactions. This is because the dyad molecules are large polymer possessing the rigid spacers to restrict the local conformational motions. According to the triplet ESPT theory, the fine structure of the spin-polarized CS state is affected by the anisotropies of the ISC and by the zero-field splitting (ZFS) interaction in the precursor triplet states.[34,35] We have applied the triplet ESPT model to reproduce the spectra, taking into account the spin polarization of the precursor excitons of $^3$P3HT*-Ph$_m$-C$_{60}$.[35] For this, we have observed a low-temperature TREPR of the triplet exciton[40] in regiorandom-P3HT (RRa-P3HT) as reported in Figure S9 of Supporting Information.

**Geometries of the Intramolecular CS States.** The triplet sublevel populations ($\rho_{11}^0$, $\rho_{22}^0$, $\rho_{33}^0$) in $T_1$, $T_2$, and $T_3$ of $^3$P3HT* generated by the ISC are transferred to $T_+$, $T_0$, and $T_-$ in the CS state as shown in Figure 3. These populations are computed by a transformation matrix $\boldsymbol{U}_{ESPT}$ which converts the spin eigen functions from ($T_1$, $T_2$, $T_3$) to ($T_+$, $T_0$, $T_-$) in the presence of the external magnetic field ($B_0$).[35] Furthermore, the energy levels of the SCRP spin functions (Figure 3) are influenced by the anisotropic $D'$ coupling and thus are dependent on the molecular conformations, i.e., the direction of the dipolar interspin vector (the orange arrow in Figure 4) between P3HT$^{+\bullet}$ and C$_{60}^{-\bullet}$ in the principal axis system ($X$, $Y$, $Z$) of the triplet exciton in Figure 4.[35] Therefore, the spin-polarized EPR spectrum is affected by the molecular geometry of the CS state, when the $D'$ coupling is effective as shown in Figure 5. To characterize the geometries and the electronic couplings of the primary CS states before the charge-dissociations, we have computed the spin-polarized EPR spectra at $t$ = 0.6 $\mu$s (Figure 2b) on the basis of the model in Figure 3. The direction of the interspin vector has been set by the $\theta$ and $\phi$ angles with respect to the principal axes of the $g$-tensor in C$_{60}^{-\bullet}$ in the present study. Accordingly, the ZFS tensor is obtained using the rotation matrix characterized by

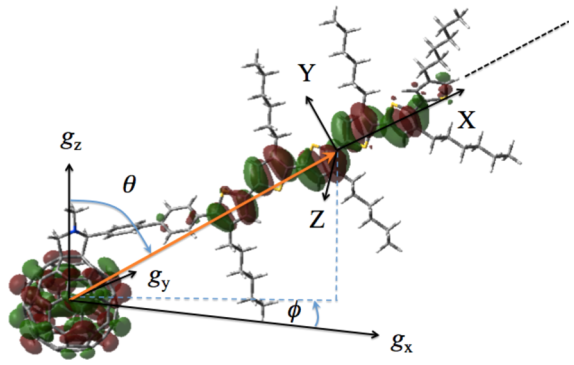


**Figure 4.** Geometry model of the primary CS state in P3HT-Ph$_2$-C$_{60}$. The principal axes of the $g$-tensor ($g_x$, $g_y$, $g_z$) and the ZFS tensor ($X$, $Y$, $Z$) are shown. The $g$-tensor orientation ($g_X$, $g_Y$, $g_Z$) in P3HT$^{+\bullet}$ was set to be colinear with the principal axes of the ZFS tensor in $^3$P3HT*. The location of the hole (P3HT$^{+\bullet}$) in the CS state is set to be the same as that of the precursor triplet exciton ($^3$P3HT*). Nonzero electronic density is identified at −Ph− in vicinity to P3HT$^{+\bullet}$, representing the hybridization of SOMO in the P3HT moiety with HOMO in the oligo-$p$-phenylene spacer.

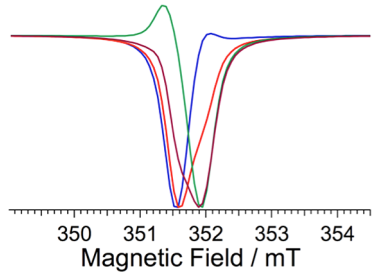


**Figure 5.** Computed TREPR spectra at $t$ = 0.6 $\mu$s for P3HT$^{+\bullet}$-Ph$_1$-C$_{60}^{-\bullet}$ by the ESPT model for different angle parameters of $\phi$ = 0° (blue), $\phi$ = −14° (red), $\phi$ = −45° (green), and $\phi$ = −90° (purple) in Figure 4. The other EPR parameters are listed in Table 1. The red spectrum is identical with the red line for $m$ = 1 in Figure 2b.

Euler angles ($\alpha$, $\beta$, $\gamma$) with respect to the principal $g$-axes in C$_{60}^{-\bullet}$. When the triplet-exciton diffusion and the subsequent charge-dissociation following the primary CS occur, the spin relaxation is expected to be much faster in the precursor triplet state than in the SCRP because of the fluctuation of the larger ZFS interaction in the triplet-exciton at the polymer backbones. Therefore, to calculate the ESPs in the exciton and in the SCRP of the dyads, the spin−lattice relaxation times of $T_{1T}$ = 20 ns and of $T_1$ = 0.6 $\mu$s (vide infra) have been utilized in the precursor triplet states and in the SCRP, respectively. The theory and computation methods on the treatments of $T_{1T}$ and $T_1$ are described in Supporting Information. The connections between the spin relaxations and the charge-dissociation motions will be detailed below.

The microwave transitions (transverse magnetizations, $\rho_{0+}$ and $\rho_{-0}$ as shown by the dark blue arrows in Figure 3) of the SCRP were previously formulated as coupled forms composed of the allowed ($T_0$−$T_\pm$) and forbidden (S−$T_\pm$) transitions, as described by eqs S26 and S27 in Supporting Information.[27,41] The EPR transition fields are dependent on the energies of $J$ and $d = D'(1 - \cos^2 \theta_B/3)/2$ in Figure 3, where $D'$ and $\theta_B$ are the dipolar coupling constant and the angle between the interspin vector and $B_0$, respectively. We have introduced the transverse relaxation times ($T_{2d}$* and $T_{2J}$*)[41] originating from heterogeneities in energies of $3d$ and $d$ −$2J$ for the $T_0$−$T_\pm$ and


DOI: 10.1021/jacs.5b13414
J. Am. Chem. Soc. 2016, 138, 5879−5885

**Table 1. EPR Parameters for the Calculations (Red Lines in Figure 2b) of the TREPR Spectra of the Photoinduced CS States in the Dyads at $t$ = 0.6 $\mu$s**

| $m$ | $D'$/mT | $J$/mT | $k_{CST}/10^7$ s$^{-1}$[a] | $T_{2d}$*/ns $T_{2J}$*/ns[b] | dipolar angles[c] | Euler angles[d] | $r_{CC}$/nm | $\|V_{CR}\|$/cm$^{-1}$ |
|---|---|---|---|---|---|---|---|---|
| 0 | −0.45 (±0.05) | >3 | 10 | 26<br>10 | $\theta$ = 54°<br>$\phi$ = −13° | $\alpha$ = 20°<br>$\beta$ = 18°<br>$\gamma$ = −5° | 1.8 | - |
| 1 | −0.38 (±0.05) | >3 | 3.1 | 40<br>12 | $\theta$ = 74°<br>$\phi$ = −14° | $\alpha$ = 34°<br>$\beta$ = 90°<br>$\gamma$ = 3° | 1.9 | - |
| 2 | −0.34 (±0.05) | 1.0 (±0.1) | 1.5 | 40<br>15 | $\theta$ = 44°<br>$\phi$ = 24° | $\alpha$ = −20°<br>$\beta$ = −80°<br>$\gamma$ = 26° | 2.0 | 3.7 (±0.1) |
| 3 | −0.20 (±0.1) | 0.6 (±0.1) | 0.7 | 40<br>12 | $\theta$ = 84°<br>$\phi$ = 4° | $\alpha$ = 10°<br>$\beta$ = 90°<br>$\gamma$ = 0° | 2.4 | 2.9 (±0.1) |

[a]CS rate constant from the triplet exciton assuming that the spin−lattice relaxation time of $T_{1T}$ is 20 ns in the triplet state. [b]Spin−spin relaxation times ($T_2$*) originating from heterogeneities in the energies of 3$d$ and $d$ − 2$J$ for the $T_0$−$T_\pm$ transition and for the S−$T_\pm$ transition in the SCRP, respectively. $d = D'(1 - \cos^2\theta_B/3)/2$, where $\theta_B$ is the angle between the interspin vector and $B_0$. [c]Direction of the dipolar principal axis between P3HT$^{+\bullet}$ and $C_{60}^{-\bullet}$ defined by the polar angles with respect to the principal $g$-tensor axes in $C_{60}^{-\bullet}$ as shown in Figure 4. Errors are ±5°. [d]Euler angles ($x$-convention) of the principal axis system ($X$, $Y$, $Z$) of $^3$P3HT* with respect to the $g$-axis system in $C_{60}^{-\bullet}$. Errors are ±2°.

S−$T_\pm$ transitions, respectively as shown in Supporting Information. It is thus anticipated that $T_{2J}$* is smaller than $T_{2d}$* when $J$ is stronger than $D'$. These two relaxation times ($T_{2d}$* = 40 ns and $T_{2J}$* = 15 ns) have first been obtained by fitting the entire spectrum shapes for $m$ = 2 and 3 in Figure 2b. Such distorted spectrum shapes largely originate from $J$ in the primary CS states (vide infra). Also, the microwave-induced S−$T_\pm$ transitions are broadened by modulations (or fast $T_{2J}$*) in the $J$ couplings because of the charge-dissociation motions at the 0.6 $\mu$s windows. $T_{2d}$* = 40 ns denotes that the dipolar term of 3$d$ is inhomogeneously distributed with a width of $1/(2\pi T_{2d}^*)$ = 4 MHz. On the other hand, the smaller $T_{2J}$* of 15 ns denotes that the 2$J$ values are more distributed with a width of 10 MHz (corresponding to a 0.4 mT variation centered at 2$J$ = ca. 2 mT) because of the effective $J$ modulation[42,43] by the charge motions. While the strength of the spin−spin dipolar coupling is not significantly affected by the small distribution in the distance, the electronic coupling between the charges is significantly modulated by such distance variation. $T_{2J}$* < $T_{2d}$* is thus reasonably explained by the effect of the above charge-dissociations. Since the dissociation motions also occur for $m$ = 0 and $m$ = 1 from Figure 2a, the similar $T_{2J}$* values were utilized. Table 1 summarizes the EPR parameters to reproduce the spectra at 0.6 $\mu$s in Figure 2b.

Figure 5 shows computed TREPR spectra at $t$ = 0.6 $\mu$s of P3HT$^{+\bullet}$-Ph$_1$-$C_{60}^{-\bullet}$ by the ESPT model for different angle parameters of $\phi$. Since the ESP is highly dependent on the conformation parameters, we have first performed the density function theory (DFT) calculation with RB3LYP/6-31G* for the dyads with taking into account hexa hexyl-thiophene rings ($n$ = 6) in the P3HT regions to obtain the optimized structures, as shown in Figures 4 and S10. From these geometry optimizations, the five angle parameters ($\theta$, $\phi$, $\alpha$, $\beta$, $\gamma$) were first predicted and were utilized as initial geometries for the fitting procedures. The resultant five angles ($\theta$, $\phi$, $\alpha$, $\beta$, $\gamma$) to fit the spectra in Figure 2b were compatible with the DFT calculations in Figure S10. There are alternate combinations of the five angle parameters to reproduce the EPR spectra even though the spectrum shapes are highly dependent on the angles. However, the positions and the orientations of the aromatic planes of the hexyl-thiophene rings in vicinity to the spacer units are expected to be firmly defined with respect to the $g_x$−$g_y$−$g_z$ axis system in $C_{60}$ because of the rigidly linked dyad by the oligo-$p$-phenylenes, as demonstrated in Figures 4 and S10. Thus, one can conclude that the agreements by the calculated red lines in Figure 2b are enough to determine the geometries of the CS states, since the angles in Table 1 are well compatible with the geometries predicted by the DFT optimizations.

From the $D'$ values in Table 1, we have obtained the center-to-center separations ($r_{CC}$) between the electron spins in the CS states using the point-dipole approximation. When the point-dipole approximation is not applicable, it is required that one takes into account the spin density distributions to obtain $r_{CC}$ from the $D'$ value. Since the distributions weaken the dipolar coupling, the distance would be smaller than $r_{CC}$ in Table 1. In fact, the spin distribution length is unknown in the CS state in Figure 4. Thus, one is unable to evaluate the accuracy in the distances, although there exist the errors in the parameter of the dipolar coupling in Table 1. Nevertheless, $r_{CC}$ ≤ 2.0 nm estimated for $m$ = 2 is well consistent with the center-to-center distance between the HOMO and the LUMO computed for $n$ = 6 in the ground state, as shown in Figure 4. This strongly supports that the primary CS states are generated by the bridge-mediated ET processes via $^3$P3HT*-Ph$_m$-$C_{60}$ when the triplet excitons reside in close proximity to the oligo-$p$-phenylene spacers.

**Electronic Couplings of the Primary CS States.** The EPR transitions are affected by two magnetic energies obtained from a sum and a difference ($Q_+$ and $Q_-$, respectively) in the Zeeman and hyperfine interactions by the individual charges as $2Q_+ = \{g_{P3HT}(\mathbf{\Omega}) + g_{C60}(\mathbf{\Omega})\}\beta B_0 + \sum_i A_{P3HT}(\mathbf{\Omega})_i M_i + \sum_j A_{C60}(\mathbf{\Omega})M_j$ and $2Q_- = \{g_{P3HT}(\mathbf{\Omega}) - g_{C60}(\mathbf{\Omega})\}\beta B_0 + \sum_i A_{P3HT}(\mathbf{\Omega})_i M_i - \sum_j A_{C60}(\mathbf{\Omega})_j M_j$, where $\mathbf{\Omega}$, $A_l$, and $M_k$ are the direction of $B_0$, the hyperfine coupling constants, and the nuclear spin quantum number in the SCRP, respectively.[15] From the McConnell relation, $A_{P3HT,xx} = 0.5A_H^{iso}$, $A_{P3HT,yy} = 1.5A_H^{iso}$, and $A_{P3HT,zz} = A_H^{iso}$ with $A_H^{iso} = Q_a\rho_C$ were used as the principal values by substituting $Q_a$= −2.5 mT and the spin densities of $\rho_C$ = 0.0431 for eight $\alpha$-protons in P3HT$^{+\bullet}$,[27] as detailed in Supporting Information. $A_{C60}(\mathbf{\Omega})$ = 0 can be set for the radical anion. Thus, the averaged value of $|Q_-|$ is ca. 0.4 mT.



DOI: 10.1021/jacs.5b13414
J. Am. Chem. Soc. 2016, 138, 5879−5885

For $m$ = 0 and 1, absolute magnitudes of the $J$ have been treated to be $|J| \gg |Q_-|$ to reproduce the TREPR spectra in Figure 2b. For $m$ = 2 and 3 at 0.6 $\mu$s, it was required to set the $J$ values of 1.0 and 0.6 mT, respectively, to reproduce the distorted spectrum shapes arising from the coherent $Q_-$-induced mixings between S and $T_0$ energetically separated by $2J + 2d$ in Figure 3.[15] From the $J$ values in the CS states, one can estimate the electronic couplings ($V_{CR}$) for the charge-recombination (CR) process, since the $2J$ in the CS state is induced by the singlet destabilization by the electronic perturbation from the ground state.[44,45]

To characterize the CR processes, time-profiles of the TREPR signals are displayed in Figure 6 at the center field

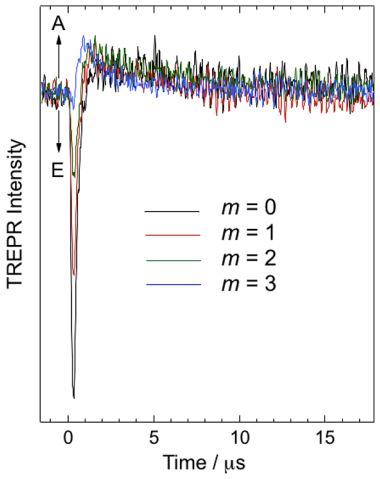


**Figure 6.** Time profiles of the TREPR signals at the center field positions (351.8 mT) in Figure 2b for the spacers of $-Ph_0-$ (black), $-Ph_1-$ (red), $-Ph_2-$ (green), and $-Ph_3-$ (blue) in P3HT$^{+\bullet}$-Ph$_m$-C$_{60}^{-\bullet}$.

positions in Figure 2b for the different spacer lengths. One finds that the initial emissive spin polarizations decay with the lifetimes of 0.6 $\mu$s attributed to $T_1$ = 0.6 $\mu$s described above, generating the weak absorptive EPR signals by the thermal equilibrium spin populations in Figures 2a and 6. Such $T_1$ effect is included in the spectrum analyses (Figure 2b) together with the S−$T_0$ relaxation time ($T_{23}$) in Figure 3 assuming $T_{23} = T_1$. The absorptive signal for >1 $\mu$s corresponds to the sharp peaks at the later delay times in Figure 2a. Slow decays ($\tau_{RP}$> 4 $\mu$s as the lifetimes in Figure 6) of the absorptive signals are attributed to radical pair deactivations via the singlet manifold after the triplet-singlet spin conversions. However, these decays are essentially independent of the spacer length. This denotes that the radical-pair deactivations are not controlled by the primary CR kinetics but by the diffusion of the holes migrating within the conjugated polymer chains in the dyads, strongly supporting the charge dissociations after the primary CSs. In the presence of $B_0$, since the triplet-singlet ($T_{\pm}$−S) conversions are highly inhibited by the Zeeman splitting after the triplet CS in Figure 3, the singlet CR is insufficient, contributing to the long-lived CS-state observations with accompanying the charge-dissociation. On the other hand, it is expected that $B_0$ = 0 will lead to the effective singlet CR after the more efficient T−S spin conversions than in the case of $B_0$ = 352 mT. Quick decays ($\tau_{RP}$ = 0.5 $\mu$s in Figure S8) of the transient absorption signals obtained in the absence of the $B_0$ are consistent with this prediction. The above magnetic field effects on the radical-pair lifetimes strongly support the triplet-precursor charge-generations in Figure 3 and the diffusion-controlled singlet CRs. Although the singlet recombination kinetics are hidden by the effects of the T−S mixings and by the charge-migrations, one is able to characterize the coupling term of $|V_{CR}|$ by using $2J = |V_{CR}|^2/\Delta E$ for the singlet CR to the ground state.[44] $\Delta E = -\Delta G_{CR} - \lambda$ is a vertical energy gap between the CS and the ground states described by the free energy change ($-\Delta G_{CR} \approx$ 1.6 eV) and by the reorganization energy ($\lambda$ = 0.6 eV) as detailed in Figure S11 in Supporting Information. $|V_{CR}|$ = 3.7 and 2.9 cm$^{-1}$ have been determined for $m$ = 2 ($r_{CC}$ = 2.0 nm) and 3 ($r_{CC}$ = 2.4 nm), respectively, as shown in Table 1. The validities of the $|V_{CR}|$ couplings are obtained by comparing them with reported couplings in corresponding bridged dyad molecules, as detailed in Supporting Information.[46,47]

In regioregular (RR)-P3HT:PCBM BHJ blend films, $|V_{CR}| \approx$ 0.2 cm$^{-1}$ was reported for the photoinduced, interfacial CS states around $r_{CC}$ = 1.8 nm.[24] Such small electronic interactions were explained by the highly delocalized intermolecular hole distributions in the crystalline phase at the D:A domain interface.[12] The quite *larger* electronic couplings of $|V_{CR}|$ > 2 cm$^{-1}$ in the present systems are thus highlighting the role of the molecular environments on the efficient charge-dissociations by the BHJ films. Comparing with the BHJ interfaces, the P3HT polymer chain is disordered and cannot form the $\pi$−$\pi$ stacking crystalline phase in the THF solution, as described in Supporting Information with Figure S12. Thus, the localized hole is generated and strengthens the bridge-mediated orbital overlap in the present CS state, as shown in Figure 4.

**Hole-Dissociation Mechanisms after Primary CS.** The solute concentration is too low ($10^{-4}$ M) to cause the submicrosecond intermolecular hole-transfer (P3HT$^{+\bullet}$-Ph$_m$-C$_{60}^{-\bullet}$ + P3HT-Ph$_m$-C$_{60}$ → P3HT-Ph$_m$-C$_{60}^{-\bullet}$ + P3HT$^{+\bullet}$-Ph$_m$-C$_{60}$) by the translational diffusion of the polymers. Thus, the intramolecular hole dissociation with $k_{diss} \approx 1\ \mu s^{-1}$ in Figure 3 is conclusive to generate the uncoupled electron−hole pairs at 1.2 $\mu$s in Figure 2a. Such intrachain hole migration after the photoinduced CS has been reported in doped poly(*N*-vinylcarbazole), although the dissociation mechanism is not fully understood.[10,11] $k_{diss} \approx 1\ \mu s^{-1}$ is in line with (1) $T_1$ = 0.6 $\mu$s obtained by decays of the $E$ signals in Figure 6 and with (2) $T_{23}$ = 0.6 $\mu$s, as the S−$T_0$ dephasing time detailed in Supporting Information, since the hole migration can induce the fluctuation in $J$ and $D$ to contribute to the population relaxations.[12,48] In Figure 6, it is seen that decay rate of the emissive polarization is not strongly affected by the spacer length, indicating that $k_{diss}$ is not modulated by the spacer.

The intramolecular hole dissociation rate of $10^6$ s$^{-1}$ is substantially smaller than the primary CS rates of $k_{CST} > 10^7$ s$^{-1}$ in Table 1. This implies that the electronic energy of the primary CS state is close to $-\Delta G_{CR} \approx 1.6$ eV of the dissociated pair of the charges, indicating that the primary CS takes place exothermically by $\Delta G_{CST} \approx -0.1$ eV as the free energy change, as shown in Figure 3. In the RR-P3HT:PCBM BHJ blend films, it is known that the electron−hole dissociation is rapid,[14,49] generating the highly delocalized electron and hole distributions within subnanosecond regimes.[4,5,7] Recent studies suggested that the crystalline phases play key roles to generate highly separated carriers in the electron−hole pairs at the D:A domain interfaces by the self-organization structures; an enthalpy stabilization ($\Delta H$ < 0) by the delocalized orbitals facilitates the three-dimensional carrier separations from the initially bound localized CT state, overcoming the Coulomb


DOI: 10.1021/jacs.5b13414
J. Am. Chem. Soc. 2016, 138, 5879−5885

binding energy ($\Delta H_C > 0$).[12,14,24] The lack of such self-organization in the present system is consistent with the slower dissociation kinetics, since the polymer chains are too disordered to produce the interchain hole delocalization in P3HT. Nevertheless, the hole distribution-length that explains $r_{CC} \leq 2.0$ nm from the dipolar coupling is shorter ($\approx 5$ thiophene rings in Figure 4) than reported delocalization lengths exceeding eight thiophene rings in a polymer molecule as studied by the pulse radiolysis[50] and by the EPR[36] for free polarons in polyalkylthiophenes. Since the localized hole distribution in Figure 4 lowers the unpaired orbital level of the hole in the primary CS state, the CS state needs to be more destabilized by ca. 0.1 eV[50] than the dissociated pair of the anion and the delocalized polaron when the Coulomb binding energy is ignored. The localized hole distribution and the large electronic-coupling in the primary CS state are both explained by the Coulomb attraction[51] between the hole in P3HT and the electron in $C_{60}$. The hybridization of the singly occupied molecular orbital (SOMO) in the P3HT moiety with the HOMO in the oligo-*p*-phenylene unit will also cause the hole distribution situated closer to $C_{60}$ in Figure 4. This hybridization effect is seen by the nonzero electronic density at the spacer unit in vicinity to $P3HT^{+\bullet}$ in Figure 4. Importantly, such hybridization of the SOMO with the HOMO in the phenylene unit will raise the localized orbital level in Figure 4, compensating for the above-mentioned lowered orbital level by the localized hole with respect to the fully delocalized free polaron. This well agrees with the above electronic energy of the primary CS state comparable to $-\Delta G_{CR} \approx 1.6$ eV for the dissociated charges. From these orbital characteristics, the $\Delta H$ stabilization would be minor (i.e., $\Delta H \approx 0$) for the intrachain hole-transfer to give rise to the more delocalized holes in the highly separated electron−hole pairs because of the hybridized SOMO in the primary CS state.

Alternatively, the polymer-chain dynamics was also discussed to play a role for the dissociations; the electron−phonon (EP) coupling may generate the delocalized hole distribution to contribute to an enhancement in the entropy ($\Delta S > 0$) with respect to the contact CT state, resulting in the one-dimensional dissociation overcoming the $\Delta H_C$ in the primary CS state.[12,24,52] In the present system, such positive $\Delta S$ may induce the exothermic intrachain hole dissociation, as expressed by $\Delta G_{diss} = \Delta H + \Delta H_C - T\Delta S < 0$. In the present primary CS state with $r_{CC} \approx 2.0$ nm, $\Delta H_C \approx 0.1$ eV is evaluated using the dielectric constant of THF ($\varepsilon_S = 7.5$). Such an electrostatic binding which energy is four times larger than the thermal energy ($k_BT$) can be overcome for $\Delta S > 30$ J $mol^{-1}$ $K^{-1}$ corresponding to the increased number ($\Delta W > 50$) of the librational states from the Boltzmann equation: $\Delta S = k_B \ln(\Delta W)$. Analysis of temperature dependence of the dissociation rate is required to clarify the roles of $\Delta S$ and $\Delta H$, which is out of scope in the present study. However, $\Delta W > 50$ predicted above is reasonable range since some of the disordered hexyl side chains ($C_6H_{13}-$) can participate in the entropy enhancement for the intrachain hole-transfer through the EP coupling.[41] The electrostatic binding energy of $\Delta H_C$ in the primary CS state needs to be dependent on the spacer length since $r_{CC}$ is dependent on *m* in Table 1. However, the hole-dissociation and migration motions are independent of the spacer length in the present system, as described above with Figure 6. Thus, the entropy effect by the disordered side chains would play a dominant role for the electron−hole dissociations.

## CONCLUSIONS

To clarify how the molecular environments play roles for the efficient initial charge-dissociations by the OPV related materials, we have investigated the orbital geometries, the electronic couplings, and the one-dimensional hole dissociation dynamics of the photoinduced intramolecular CS states in the P3HT-$Ph_m$-$C_{60}$ dyads using the TREPR. It has been clearly demonstrated that the hole dissociation takes place without going through the hot CT state; the localized hole is initially generated in the conjugated polymer region nearby the phenylene-bridge unit by the bridge-mediated electron tunneling via the triplet excitons. The entropy enhancement by the disordered side chains may play a major role to induce the one-dimensional hole-dissociation via the hybridized SOMOs in Figure 4. The present thermodynamic dissociation mechanism (as opposed to the hot CT mechanism) would be characteristic to the triplet-precursor reaction systems, since the long-lived triplet excitons are generated after the vibrational relaxations. Although the charge dissociation is slower than in the BHJ photoactive layers due to the lack of the $\pi-\pi$ stacking interactions, the present molecular-wire property[53] may pave a new avenue to rational designs of the efficient molecular electronics using the bridged polymer molecules.

## ASSOCIATED CONTENT

### Supporting Information

The Supporting Information is available free of charge on the ACS Publications website at DOI: 10.1021/jacs.5b13414.

Synthesis of P3HT-$Ph_m$-$C_{60}$ and their characterizations, experimental details, the ESPT theory, and the computation methods (PDF)

## AUTHOR INFORMATION


### Corresponding Authors

*E-mail: imahori@scl.kyoto-u.ac.jp

*E-mail: ykobori@kitty.kobe-u.ac.jp


### Notes

The authors declare no competing financial interest.

## ACKNOWLEDGMENTS

This work was supported by a Grant-in-Aid for Scientific Research (Nos. 25288004 and 26620065 to Y.K. and 25220801 to H.I.) from the Ministry of Education, Culture, Sports, Science and Technology, Japan.

## REFERENCES


(1) Balabin, I. A.; Onuchic, J. N. *Science* **2000**, *290*, 114−117.

(2) Yu, G.; Gao, J.; Hummelen, J. C.; Wudl, F.; Heeger, A. J. *Science* **1995**, *270*, 1789−1791.

(3) Kraffert, F.; Steyrleuthner, R.; Albrecht, S.; Neher, D.; Scharber, M. C.; Bittl, R.; Behrends, J. *J. Phys. Chem. C* **2014**, *118*, 28482−28493.

(4) Guo, J. M.; Ohkita, H.; Benten, H.; Ito, S. *J. Am. Chem. Soc.* **2010**, *132*, 6154−6164.

(5) Bakulin, A. A.; Rao, A.; Pavelyev, V. G.; van Loosdrecht, P. H. M.; Pshenichnikov, M. S.; Niedzialek, D.; Cornil, J.; Beljonne, D.; Friend, R. H. *Science* **2012**, *335*, 1340−1344.

(6) Lee, J.; Vandewal, K.; Yost, S. R.; Bahlke, M. E.; Goris, L.; Baldo, M. A.; Manca, J. V.; Van Voorhis, T. *J. Am. Chem. Soc.* **2010**, *132*, 11878−11880.

(7) Tamura, H.; Burghardt, I. *J. Am. Chem. Soc.* **2013**, *135*, 16364−16367.

(8) Grancini, G.; Maiuri, M.; Fazzi, D.; Petrozza, A.; Egelhaaf, H. J.; Brida, D.; Cerullo, G.; Lanzani, G. *Nat. Mater.* **2013**, *12*, 29−33.




DOI: 10.1021/jacs.5b13414
*J. Am. Chem. Soc.* 2016, 138, 5879−5885

(9) Vandewal, K.; Albrecht, S.; Hoke, E. T.; Graham, K. R.; Widmer, J.; Douglas, J. D.; Schubert, M.; Mateker, W. R.; Bloking, J. T.; Burkhard, G. F.; Sellinger, A.; Frechet, J. M. J.; Amassian, A.; Riede, M. K.; McGehee, M. D.; Neher, D.; Salleo, A. *Nat. Mater.* **2014**, *13*, 63−68.
(10) Miyasaka, H.; Moriyama, T.; Itaya, A. *J. Phys. Chem.* **1996**, *100*, 12609−12615.
(11) Ito, F.; Ikoma, T.; Akiyama, K.; Kobori, Y.; Tero-Kubota, S. *J. Am. Chem. Soc.* **2003**, *125*, 4722−4723.
(12) Kobori, Y.; Miura, T. *J. Phys. Chem. Lett.* **2015**, *6*, 113−123.
(13) Pensack, R. D.; Guo, C.; Vakhshouri, K.; Gomez, E. D.; Asbury, J. B. *J. Phys. Chem. C* **2012**, *116*, 4824−4831.
(14) Grzegorczyk, W. J.; Savenije, T. J.; Dykstra, T. E.; Piris, J.; Schins, J. M.; Siebbeles, L. D. A. *J. Phys. Chem. C* **2010**, *114*, 5182−5186.
(15) Closs, G. L.; Forbes, M. D. E.; Norris, J. R. *J. Phys. Chem.* **1987**, *91*, 3592−3599.
(16) Hore, P. J.; Hunter, D. A.; McKie, C. D.; Hoff, A. J. *Chem. Phys. Lett.* **1987**, *137*, 495−500.
(17) Norris, J. R.; Morris, A. L.; Thurnauer, M. C.; Tang, J. *J. Chem. Phys.* **1990**, *92*, 4239−4249.
(18) Kothe, G.; Weber, S.; Bittl, R.; Ohmes, E.; Thurnauer, M. C.; Norris, J. R. *Chem. Phys. Lett.* **1991**, *186*, 474−480.
(19) Prisner, T. F.; Vanderest, A.; Bittl, R.; Lubitz, W.; Stehlik, D.; Mobius, K. *Chem. Phys.* **1995**, *194*, 361−370.
(20) vanderEst, A.; Prisner, T.; Bittl, R.; Fromme, P.; Lubitz, W.; Mobius, K.; Stehlik, D. *J. Phys. Chem. B* **1997**, *101*, 1437−1443.
(21) Lukina, E. A.; Popov, A. A.; Uvarov, M. N.; Kulik, L. V. *J. Phys. Chem. B* **2015**, *119*, 13543−13548.
(22) Bittl, R.; Weber, S. *Biochim. Biophys. Acta, Bioenerg.* **2005**, *1707*, 117−126.
(23) Franco, L.; Ruzzi, M.; Corvaja, C. *J. Phys. Chem. B* **2005**, *109*, 13431−13435.
(24) Kobori, Y.; Noji, R.; Tsuganezawa, S. *J. Phys. Chem. C* **2013**, *117*, 1589−1599.
(25) Scott, A. M.; Miura, T.; Ricks, A. B.; Dance, Z. E. X.; Giacobbe, E. M.; Colvin, M. T.; Wasielewski, M. R. *J. Am. Chem. Soc.* **2009**, *131*, 17655−17666.
(26) Poluektov, O. G.; Paschenko, S. V.; Utschig, L. M.; Lakshmi, K. V.; Thurnauer, M. C. *J. Am. Chem. Soc.* **2005**, *127*, 11910−11911.
(27) Kobori, Y.; Ponomarenko, N.; Norris, J. R. *J. Phys. Chem. C* **2015**, *119*, 8078−8088.
(28) Carmieli, R.; Smeigh, A. L.; Conron, S. M. M.; Thazhathveetil, A. K.; Fuki, M.; Kobori, Y.; Lewis, F. D.; Wasielewski, M. R. *J. Am. Chem. Soc.* **2012**, *134*, 11251−11260.
(29) Barker, A. J.; Chen, K.; Hodgkiss, J. M. *J. Am. Chem. Soc.* **2014**, *136*, 12018−12026.
(30) Fujitsuka, M.; Masuhara, A.; Kasai, H.; Oikawa, H.; Nakanishi, H.; Ito, O.; Yamashiro, T.; Aso, Y.; Otsubo, T. *J. Phys. Chem. B* **2001**, *105*, 9930−9934.
(31) Banerji, N.; Seifter, J.; Wang, M. F.; Vauthey, E.; Wudl, F.; Heeger, A. J. *Phys. Rev. B: Condens. Matter Mater. Phys.* **2011**, *84*, 075206.
(32) Poluektov, O. G.; Filippone, S.; Martin, N.; Sperlich, A.; Deibel, C.; Dyakonov, V. *J. Phys. Chem. B* **2010**, *114*, 14426−14429.
(33) Atkins, P. W.; Evans, G. T. *Mol. Phys.* **1974**, *27*, 1633−1644.
(34) Kobori, Y.; Fuki, M. *J. Am. Chem. Soc.* **2011**, *133*, 16770−16773.
(35) Kobori, Y.; Fuki, M.; Murai, H. *J. Phys. Chem. B* **2010**, *114*, 14621−14630.
(36) Marumoto, K.; Takeuchi, N.; Kuroda, S. *Chem. Phys. Lett.* **2003**, *382*, 541−546.
(37) Monkman, A. P.; Burrows, H. D.; Hartwell, L. J.; Horsburgh, L. E.; Hamblett, I.; Navaratnam, S. *Phys. Rev. Lett.* **2001**, *86*, 1358−1361.
(38) Hsu, H. Y.; Vella, J. H.; Myers, J. D.; Xue, J. G.; Schanze, K. S. *J. Phys. Chem. C* **2014**, *118*, 24282−24289.
(39) Fujisawa, J.; Ohba, Y.; Yamauchi, S. *J. Am. Chem. Soc.* **1997**, *119*, 8736−8737.
(40) Biskup, T.; Sommer, M.; Rein, S.; Meyer, D. L.; Kohlstadt, M.; Wurfel, U.; Weber, S. *Angew. Chem., Int. Ed.* **2015**, *54*, 7707−7710.
(41) Miura, T.; Aikawa, M.; Kobori, Y. *J. Phys. Chem. Lett.* **2014**, *5*, 30−35.
(42) Avdievich, N. I.; Forbes, M. D. E. *J. Phys. Chem.* **1995**, *99*, 9660−9667.
(43) Avdievich, N. I.; Forbes, M. D. E. *J. Phys. Chem.* **1996**, *100*, 1993−1995.
(44) Kobori, Y.; Sekiguchi, S.; Akiyama, K.; Tero-Kubota, S. *J. Phys. Chem. A* **1999**, *103*, 5416−5424.
(45) Anderson, P. W. *Phys. Rev.* **1959**, *115*, 2−13.
(46) Higashino, T.; Yamada, T.; Yamamoto, M.; Furube, A.; Tkachenko, N. V.; Miura, T.; Kobori, Y.; Jono, R.; Yamashita, K.; Imahori, H. *Angew. Chem., Int. Ed.* **2016**, *55*, 629−633.
(47) Hanss, D.; Wenger, O. S. *Eur. J. Inorg. Chem.* **2009**, *2009*, 3778−3790.
(48) Fukuju, T.; Yashiro, H.; Maeda, K.; Murai, H.; Azumi, T. *J. Phys. Chem. A* **1997**, *101*, 7783−7786.
(49) Saeki, A.; Yoshikawa, S.; Tsuji, M.; Koizumi, Y.; Ide, M.; Vijayakumar, C.; Seki, S. *J. Am. Chem. Soc.* **2012**, *134*, 19035−19042.
(50) Takeda, N.; Miller, J. R. *J. Phys. Chem. B* **2012**, *116*, 14715−14723.
(51) Niklas, J.; Mardis, K. L.; Banks, B. P.; Grooms, G. M.; Sperlich, A.; Dyakonov, V.; Beaupre, S.; Leclerc, M.; Xu, T.; Yu, L. P.; Poluektov, O. G. *Phys. Chem. Chem. Phys.* **2013**, *15*, 9562−9574.
(52) Clarke, T. M.; Durrant, J. R. *Chem. Rev.* **2010**, *110*, 6736−6767.
(53) Sukegawa, J.; Schubert, C.; Zhu, X.; Tsuji, H.; Guldi, D. M.; Nakamura, E. *Nat. Chem.* **2014**, *6*, 899−905.


DOI: 10.1021/jacs.5b13414
*J. Am. Chem. Soc.* 2016, 138, 5879−5885